

# Pseudo-Goldstone boson effects in $t\bar{t}$ productions at high energy hadron colliders and testing technicolor models

Ling Zhang<sup>b</sup>    Xue-Lei Wang<sup>abc</sup>    Yu-Ping Kuang<sup>ab</sup>    Hong-Yi Zhou<sup>ab</sup>

*a. China Center of Advanced Science and Technology (World Laboratory), P.O.Box 8730, Beijing 100080, China*

*b. Department of Physics, Tsinghua University, Beijing 100084, China\**

*c. Physics Department, Henan Normal University, Xinxiang 453002, Henan, China*  
(TU-HEP-TH-99/103)

We study the top quark pair production process  $pp(\bar{p}) \rightarrow t\bar{t}$  in various kinds of technicolor (TC) models at the Fermilab Tevatron Run II and the CERN LHC. The s-channel neutral pseudo-Goldstone bosons (PGBs) contribute dominantly to the production amplitudes from its coupling to the gluons through the triangle loops of techniquarks and the top quark. Cross sections in different TC models with s-channel PGB contributions are calculated. It is shown that the PGB effects can be experimentally tested and different TC models under consideration can be distinguished at the LHC. Therefore, the  $pp \rightarrow t\bar{t}$  process at the LHC provides feasible tests of technicolor models.

PACS number(s): 12.15.Lk, 12.60.Nz, 13.30.Eg

## I. INTRODUCTION

Understanding the mechanism of electroweak symmetry breaking (EWSB) is one of the most important problems in current particle physics and will be studied experimentally at present and future high energy colliders, for instance the CERN LEP2 and LHC, the Fermilab Tevatron Run II, and the future  $e^+e^-$  linear colliders. The standard model (SM) Higgs boson has not been found yet, and the Higgs sector in the SM suffers from the well-known problems of *triviality* and *unnaturalness*. So that the EWSB mechanism is possibly related to new physics beyond the SM. Two main candidates of new physics related to the EWSB mechanism are supersymmetry and dynamical EWSB mechanism, for example various technicolor (TC) models.

TC models are based on new strong interaction dynamics which is difficult to deal with. However, TC models contain certain new particles, such as new heavy gauge bosons and new resonances. It is feasible to test TC models via processes including the contributions of these new particles. On the other hand, The top quark is the heaviest particle yet discovered. The directly measured top quark mass is  $m_t = 174.3 \pm 3.2 \pm 4.0$  GeV [1] which is close to the EWSB scale  $v = 246$  GeV, so that the effective Yukawa coupling of the top quark is of the order of 1. Thus TC models may be detected through study-

ing new particle contributions to top quark production processes at future high energy colliders. Study of the contributions of s-channel new heavy gauge bosons and new vector-resonances (color-singlet, color-octet, or hybrid) in TC models of masses ranging from 600 GeV to 1 TeV to  $t\bar{t}$  productions at the Tevatron has been given in Ref. [2], which shows that the effects are experimentally detectable. Another characteristic feature of the TC models is that most TC models predict certain pseudo-Goldstone bosons (PGBs) of masses below 1 TeV, and the properties of the PGBs are different in different models. Therefore, studying the effects of the PGB contributions in  $t\bar{t}$  productions at high energy colliders can serve as good tests of TC models. The effect of color-octet technipions  $\Pi^{0a}$  ( $a = 1, \dots, 8$ ) on  $t\bar{t}$  production at the Fermilab Tevatron has been studied in Ref. [3] and it shows that  $\Pi^{0a}$  can make important contributions via the gluon fusion process  $gg \rightarrow \Pi^{0a} \rightarrow t\bar{t}$  due to the large PGB-gluon-gluon coupling contributed by the techniquark triangle-loop, and such effect can be tested by measuring the differential cross section. A more complete study of the PGB effects in the  $t\bar{t}$  productions at the Tevatron and the LHC in the topcolor-assisted multiscale TC model has been studied in Ref. [4] in which the contributions from the color-singlet technipion and the top-pion are included as well, and the total effects

are shown to be large enough to be experimentally detected. In Ref. [5], the  $\gamma\gamma \rightarrow t\bar{t}$  process at the future photon collider in various TC models (with and without topcolor) is studied. It is shown that the  $s$ -channel PGB contributions are dominant, and the results show that different TC models can be experimentally distinguished at the future photon colliders. In this paper, we extend the study of Ref. [4] to include various kinds of typical TC models as studied in Ref. [5] and examine whether those typical TC models can also be experimentally distinguished at the future hadron colliders. Since there can be  $s$ -channel color-octet PGBs contributing to the  $t\bar{t}$  productions at the hadron colliders, the present case is different from that in Ref. [5]. Our calculation will show that, with the expected systematic errors in the  $t\bar{t}$  cross section measurements at the LHC, experimentally testing and distinguishing different kinds of TC models are possible by measuring the  $t\bar{t}$  production cross section and the invariant mass distribution at the LHC. Therefore, the  $t\bar{t}$  production process provides feasible tests of technicolor models.

This paper is organized as follows. In Sec. II, we present the calculation of the production amplitudes for three typical TC models with and without topcolor. The numerical results of the production cross sections are presented in Sec. III, and a concluding remark is given in Sec. IV.

## II. CALCULATION OF THE PRODUCTION AMPLITUDES FOR THREE TYPICAL TC MODELS

We shall take into account the tree-level SM amplitude  $\mathcal{M}_{tree}^{SM}$  and the PGB contributed amplitude  $\mathcal{M}_{\Pi}$  ( $\Pi$  stands for the related PGB in this paper) described in Fig. 1. At the hadron colliders,  $\mathcal{M}_{tree}^{SM}$  mainly contains two parts, namely the quark fusion amplitude  $\mathcal{M}_{tree}^{SM}(q\bar{q} \rightarrow t\bar{t})$  and the gluon fusion amplitude  $\mathcal{M}_{tree}^{SM}(gg \rightarrow t\bar{t})$ , i.e.

$$\mathcal{M}_{tree}^{SM} = \mathcal{M}_{tree}^{SM}(q\bar{q} \rightarrow t\bar{t}) + \mathcal{M}_{tree}^{SM}(gg \rightarrow t\bar{t}). \quad (1)$$

For the LHC,  $\mathcal{M}_{tree}^{SM}(gg \rightarrow t\bar{t})$  dominates, and we shall neglect  $\mathcal{M}_{tree}^{SM}(q\bar{q} \rightarrow t\bar{t})$  in the calculation. For the Tevatron, although  $\mathcal{M}_{tree}^{SM}(q\bar{q} \rightarrow t\bar{t})$  is dominant, the interference term between  $\mathcal{M}_{tree}^{SM}(gg \rightarrow t\bar{t})$  and  $\mathcal{M}_{\Pi}$  is actually not negligibly small, so that we shall take account of both  $\mathcal{M}_{tree}^{SM}(q\bar{q} \rightarrow t\bar{t})$  and  $\mathcal{M}_{tree}^{SM}(gg \rightarrow t\bar{t})$  in our calculation. For  $\mathcal{M}_{\Pi}$ , as in Ref. [5], we take the Appelquist-Terning one family walking TC model (Model A) [6], the original topcolor-assisted technicolor model (Model B) [7] and the topcolor-assisted multiscale technicolor model (Model C) [8] as three typical examples of TC models with and without topcolor to illustrate the results. The details will be presented as follows.

### A. The Appelquist-Terning One Family Walking TC Model (Model A)

We take this model as a typical example of the improved TC models without assisted by topcolor. To reduce the value of the oblique correction parameter  $S$ , this model is designed such that the techniquark ( $Q$ ) sector respects the custodial  $SU(2)$  symmetry, while the technilepton ( $L$ ) sector is custodial  $SU(2)$  violating, and the vacuum expectation values (VEV's) of  $\bar{Q}Q$  and  $\bar{L}L$  are further designed to be  $F_Q \gg F_L$  [6]. The color-singlet would-be Goldstone bosons eaten by  $W$  and  $Z$  are mainly composed of techniquarks. There are 36 PGBs in this model [6], in which the color-singlet PGBs are mainly composed of technileptons which are irrelevant to the  $s$ -channel  $t\bar{t}$  production. At the hadron colliders, the color-octet PGBs  $\Pi^{0a}$  ( $a = 1, \dots, 8$ ) composed of techniquarks can contribute to the  $s$ -channel  $t\bar{t}$  productions via the techniquark and top quark triangle loops [cf. Fig. 1]. This is the main difference between the present case and the  $\gamma\gamma \rightarrow t\bar{t}$  case in Ref. [5]. The decay constant of the color-octet PGBs is  $F_{\Pi} = 123$  GeV [6]. The masses of  $\Pi^{0a}$  are model-dependent. Following Ref. [6], we take  $M_{\Pi^{0a}}$  in the range  $400 \text{ GeV} \lesssim M_{\Pi^{0a}} \lesssim 500 \text{ GeV}$ .

Since the techniquark  $Q$  is very heavy, the triangle loop in Fig. 1(a) can be simply evaluated by the Adler-Bell-Jackiw anomaly [9], and the general form of which is [10,11]

$$\frac{S_{\Pi^{0a} B_1 B_2}}{4\pi^2 F_{\Pi}} \epsilon_{\mu\nu\lambda\rho} k_1^{\lambda} k_2^{\rho}, \quad (2)$$

where  $B_1$  and  $B_2$  denote the two gauge fields which, in our case, are the two gluons  $g_b$  and  $g_c$  with the color indices  $b$  and  $c$ , respectively. The factor  $S_{\Pi^{0a} g_b g_c}$  can be easily obtained from the formulae in Ref. [10,11,4], and it is\*

$$S_{\Pi^{0a} g_b g_c} = \frac{1}{\sqrt{2}} g_s^2 N_{TC} d_{abc}, \quad (3)$$

where  $d_{abc}$  is the symmetric tensor in the color  $SU(3)_c$  group.

The evaluation of the triangle loop in Fig. 1(b) needs more consideration. The top quark is not heavy enough for the validity of simply using the Adler-Bell-Jackiw anomaly. Correction of the  $m_t$  effect has to be taken into account. This has been calculated in Ref. [12], and the result is

$$-i \frac{C_t g_s^2}{8\pi^2 F_{\Pi}} \frac{d_{abc}}{2} J(R_s) \epsilon_{\mu\nu\lambda\rho} k_1^{\lambda} k_2^{\rho}, \quad (4)$$

---

\*Here, and in (4), (5) and (8), we have corrected some typos in Ref. [4].

where  $C_t$  is a model-dependent coupling constant which is expected to be of order 1 [8,10,13],  $\hat{s}$  is the center-of mass energy of the  $t\bar{t}$  system and  $J(R_{\hat{s}})$  is defined as [12]

$$J(R_{\hat{s}}) \equiv -\frac{1}{R_{\hat{s}}^2} \int_0^1 \frac{dx}{x(1-x)} \times \ln[1 - R_{\hat{s}}^2 x(1-x)], \quad (5)$$

with  $R_{\hat{s}} \equiv \sqrt{\hat{s}}/m_t$ .

Combining (2), (3) and (4), we obtain the production amplitude for Fig. 1

$$\mathcal{M}_{\Pi^{0a}}^{(A)} = \frac{C_t m_t g_s^2 [N_{TC} + \frac{1}{2\sqrt{2}} C_t J(R_{\hat{s}})] d_{abc}}{4\sqrt{2}\pi^2 F_{\Pi}^2 [\hat{s} - M_{\Pi^{0a}}^2 + i M_{\Pi^{0a}} \Gamma_{\Pi^{0a}}]} \times (\bar{t} \gamma_5 \frac{\lambda_a}{2} t) \epsilon_{\mu\nu\lambda\rho} \epsilon_1^\mu \epsilon_2^\nu k_1^\lambda k_2^\rho, \quad (6)$$

where  $\Gamma_{\Pi^{0a}}$  is the total width of  $\Pi^{0a}$  which has been given in Ref. [4]. The total production amplitude is then

$$\mathcal{M}^{(A)} = \mathcal{M}_{tree}^{SM} + \mathcal{M}_{\Pi^{0a}}^{(A)}. \quad (7)$$

## B. The Original Topcolor-Assisted Technicolor Model (Model B)

Since the original topcolor-assisted technicolor model (Model B) was proposed [7], there have been refinements of the model to make it more realistic [14]. In the present study, we are only interested in the characteristic PGB effects of this kind of model in  $t\bar{t}$  productions which do not concern the subtleties of the refinements, so that we simply take the original Model B as a typical example of this kind of model in our calculation. In this model, the TC sector is taken to be the standard extended technicolor model in which there are 60 TC PGBs with the decay constant  $F_{\Pi} \approx 120 \text{ GeV}^\dagger$ , and both the color-octet PGB  $\Pi^{0a}$  and the color-singlet PGB  $\Pi^0$  contribute to the  $t\bar{t}$  production. As in Model A, we take  $400 \lesssim M_{\Pi^{0a}} \lesssim 500 \text{ GeV}$ . The mass of  $\Pi^0$  is lighter, say around  $150 \text{ GeV}$  [18]. The coupling of  $\Pi^0$  to gluons via the techniquark and top quark triangle loops is described by [10,4]

$$S_{\Pi^0 g_b g_c}^{(B)} = \frac{1}{2\sqrt{3}} g_s^2 \delta_{bc} N_{TC} + \frac{1}{\sqrt{2}} g_s^2 J(R_{\hat{s}}) \delta_{bc}, \quad (8)$$

---

<sup>†</sup>This is slightly smaller than the usual value  $F_{\Pi} = 123 \text{ GeV}$  in the extended technicolor model since, in the topcolor-assisted technicolor model, the total vacuum expectation value is also contributed by the topcolor sector.

where the first term is from the techniquark loop and the second term is from the top quark loop.

There is a topcolor sector in this model responsible for causing the main part of the top quark mass. In the topcolor sector, there is a PGB called top-pion  $\Pi_t$  with decay constant  $F_{\Pi_t} = 50 \text{ GeV}$ . The mass  $M_{\Pi_t}$  was first estimated as around  $200 \text{ GeV}$  in the original paper [7]. However, recent phenomenological analyses up to one-loop calculations show that the LEP/SLD precision data of  $R_b$  give severe constraint on the value of  $M_{\Pi_t}$  due to the large negative contribution to  $R_b$  from the corrections related to  $\Pi_t$ , and it requires  $M_{\Pi_t}$  to be of the order of  $1 \text{ TeV}$  [15,16]. However, as is pointed out in Ref. [15], such a constraint can only be regarded as a rough estimate since higher order corrections related to  $\Pi_t$  may be substantial due to the large  $\Pi_t - t - \bar{b}$  coupling. Furthermore, the extended technicolor gauge boson contribution to  $R_b$ , which has been shown to be positive [17], is not taken into account in the analyses in Refs. [15,16], and the actual constraint on  $M_{\Pi_t}$  may be relaxed when such a positive contribution is taken into account. Therefore, to see the  $M_{\Pi_t}$ -dependence of the cross section, we take  $M_{\Pi_t}$  to vary in the range  $500 \text{ GeV} \lesssim M_{\Pi_t} \lesssim 1 \text{ TeV}$  in our calculation.

The top quark mass  $m_t$  comes from two sources in this model. The TC sector gives rise to a small portion of it, and we call this portion  $m'_t$ . The value of  $m'_t$  is model-dependent. Low energy data, especially the  $b \rightarrow s\gamma$  experiment, give constraints on  $m'_t$ , and the reasonable range of  $m'_t$  is about  $5 \text{ GeV} \lesssim m'_t \lesssim 20 \text{ GeV}$  [7,19]. The rest part of  $m_t$ , say  $m_t - m'_t$  comes from the topcolor sector. Thus the couplings of the technipions to the top quark can be written as [3] [10]

$$\frac{C_t m'_t}{\sqrt{2} F_{\Pi}} \Pi^0 (\bar{q} \gamma^5 q) \quad (9)$$

$$\frac{C_t m'_t}{F_{\Pi}} \Pi^{0a} (\bar{q} \gamma^5 \frac{\lambda^a}{2} q) \quad (10)$$

where  $\lambda^a$  is the Gell-Mann matrix of the color group. The interactions of the top-pions with the top quark is [7,14]

$$\frac{m_t - m'_t}{\sqrt{2} F_{\Pi_t}} [\bar{t} \gamma_5 t \Pi_t^0 + \frac{i}{\sqrt{2}} \bar{t} (1 - \gamma_5) b \Pi_t^+ + \frac{i}{\sqrt{2}} \bar{b} (1 + \gamma_5) t \Pi_t^-]. \quad (11)$$

With these couplings, the PGB contributed production amplitudes in this model described in Fig. 1 are

$$\mathcal{M}_{\Pi^{0a}}^{(B)} = \frac{C_t m'_t g_s^2 [N_{TC} + \frac{1}{2\sqrt{2}} C_t J(R_{\hat{s}})] d_{abc}}{4\sqrt{2}\pi^2 F_{\Pi}^2 [\hat{s} - M_{\Pi^{0a}}^2 + i M_{\Pi^{0a}} \Gamma_{\Pi^{0a}}]} \times (\bar{t} \gamma_5 \frac{\lambda_a}{2} t) \epsilon_{\mu\nu\lambda\rho} \epsilon_1^\mu \epsilon_2^\nu k_1^\lambda k_2^\rho, \quad (12)$$

$$\mathcal{M}_{\Pi^0}^{(B)} = \frac{C_t m'_t g_s^2 [N_{TC} + \frac{\sqrt{6}}{2} C_t J(R_s)] \delta_{bc}}{8\sqrt{6}\pi^2 F_{\Pi^0}^2 [\hat{s} - M_{\Pi^0}^2 + iM_{\Pi^0}\Gamma_{\Pi^0}]} \times (\bar{t}\gamma_5 t) \epsilon_{\mu\nu\lambda\rho} \epsilon_1^\mu \epsilon_2^\nu k_1^\lambda k_2^\rho, \quad (13)$$

$$\mathcal{M}_{\Pi_t}^{(B)} = \frac{(m_t - m'_t) g_s^2 J(R_s) \delta_{bc}}{8\sqrt{6}\pi^2 F_{\Pi_t}^2 [\hat{s} - M_{\Pi_t}^2 + iM_{\Pi_t}\Gamma_{\Pi_t}]} \times (\bar{t}\gamma_5 t) \epsilon_{\mu\nu\lambda\rho} \epsilon_1^\mu \epsilon_2^\nu k_1^\lambda k_2^\rho, \quad (14)$$

where  $\Gamma_{\Pi^0}$  and  $\Gamma_{\Pi_t}$  are, respectively, the total widths of  $\Pi^0$  and  $\Pi_t$  given in Ref. [4]. The total production amplitude in this model is then

$$\mathcal{M}^{(B)} = \mathcal{M}_{tree}^{SM} + \mathcal{M}_{\Pi^{0a}}^{(B)} + \mathcal{M}_{\Pi^0}^{(B)} + \mathcal{M}_{\Pi_t}^{(B)}. \quad (15)$$

Compared with  $\mathcal{M}^{(A)}$ , the amplitude  $\mathcal{M}^{(B)}$  contains two extra terms  $\mathcal{M}_{\Pi^0}^{(B)}$  and  $\mathcal{M}_{\Pi_t}^{(B)}$ . As we shall see later that this makes Model A and Model B experimentally distinguishable at the LHC.

### C. The Topcolor-Assisted Multiscale Technicolor Model (Model C)

The topcolor-assisted multiscale technicolor model (Model C) [8,3,4] is different from Model B by its extended technicolor sector which is taken to be the multiscale technicolor model [20]. In this model, the value of the decay constant  $F_{\Pi}$  is  $F_{\Pi} = 40$  GeV rather than 120 GeV, and the technipion  $\Pi^0$  is almost composed of pure techniquarks (ideal mixing) [8] which leads to

$$S_{\Pi^0 g_b g_c}^{(C)} = \frac{1}{\sqrt{3}} N_{TC} \delta_{bc}. \quad (16)$$

Then the production amplitudes in Model C is

$$\mathcal{M}^{(C)} = \mathcal{M}_{tree}^{SM} + \mathcal{M}_{\Pi^{0a}}^{(C)} + \mathcal{M}_{\Pi^0}^{(C)} + \mathcal{M}_{\Pi_t}^{(C)}, \quad (17)$$

with

- $\mathcal{M}_{\Pi_t}^{(C)} = \mathcal{M}_{\Pi_t}^{(B)}$ ;
- the formula for  $\mathcal{M}_{\Pi^0}^{(C)}$  differs from that for  $\mathcal{M}_{\Pi^0}^{(B)}$  by a factor of 2;
- the value of  $F_{\Pi}$  in  $\mathcal{M}_{\Pi^{0a}}^{(C)}$  and  $\mathcal{M}_{\Pi^0}^{(C)}$  is  $F_{\Pi} = 40$  GeV rather than 123 GeV.

The smallness of the value of  $F_{\Pi}$  and the ideal mixing of  $\Pi^0$  in model C enhance the technicolor PGB contributions in  $t\bar{t}$  production relative to the top-pion contribution. As we shall see later that this makes Model C experimentally distinguishable from Model B and Model A.

## III. CROSS SECTIONS AND NUMERICAL RESULTS

We take the method in Ref. [21] to do the numerical calculation. Once the elementary cross section  $\hat{\sigma}$  is calculated at the parton-level, the total cross section  $\sigma$  can be obtained by folding  $\hat{\sigma}$  with the parton distribution functions  $f_i^{p(\bar{p})}(x_i, Q)$  [22]

$$\sigma(pp(\bar{p}) \rightarrow t\bar{t}) = \sum_{ij} \int dx_i dx_j f_i^{(p)}(x_i, Q) f_j^{(p(\bar{p}))}(x_j, Q) \times \hat{\sigma}(ij \rightarrow t\bar{t}) \quad (18)$$

where  $i$  and  $j$  stand for the partons  $g, q$  and  $\bar{q}$ ;  $x_i$  is the fraction of longitudinal momentum of the proton (antiproton) carried by the  $i$ th parton;  $Q^2 \approx \hat{s}$ ; and  $f_i^{(p(\bar{p}))}$  is the parton distribution function in the proton (antiproton). In this paper, we take the MRS setA' parton distribution for  $f_i^{p(\bar{p})}$  [23]. To take account of the QCD corrections, we shall multiply the obtained cross section by a factor of 1.6 [24] as what was done in Ref. [4]. The values of the tree-level SM cross section  $\sigma_0$  at the  $\sqrt{s} = 2$  TeV Tevatron and the  $\sqrt{s} = 14$  TeV LHC are, respectively

$$\begin{aligned} \text{Tevatron :} & \quad \sigma_0 = 8.02 \text{ pb}, \\ \text{LHC :} & \quad \sigma_0 = 826 \text{ pb}. \end{aligned} \quad (19)$$

In the numerical calculations, we take  $\alpha_s(\sqrt{\hat{s}})$  the same as that in the MRS set A' parton distributions,  $m_t = 174$  GeV, and we simply take the technicolor model parameter  $C_t = 1$ . In the following analysis, we consider the one-year-run integrated luminosities for the Tevatron Run II and the LHC

$$\begin{aligned} \text{Tevatron :} & \quad \int \mathcal{L} dt = 2 \text{ fb}^{-1}, \\ \text{LHC :} & \quad \int \mathcal{L} dt = 100 \text{ fb}^{-1}, \end{aligned} \quad (20)$$

and assume a 10% detecting efficiency.

The obtained total production cross sections can be compared with the recently measured  $t\bar{t}$  production cross sections by the CDF Collaboration and the D0 Collaboration [1]

$$\begin{aligned} \text{CDF :} & \quad \sigma(pp \rightarrow t\bar{t}) = 10.1 \pm 1.9_{-3.1}^{+4.1} \text{ pb}, \\ \text{D0 :} & \quad \sigma(pp \rightarrow t\bar{t}) = 7.1 \pm 2.8 \pm 1.5 \text{ pb}. \end{aligned} \quad (21)$$

The data in (21) can serve as a constraint on the parameters in the TC models.

### A. Results of Model A

In Table I, we list the results of the cross sections at the Tevatron Run II and the LHC in Model A with  $M_{\Pi^{0a}}$

varying from 400 GeV to 500 GeV. We see from Table I that the values of  $\sigma_{t\bar{t}}^{(A)}$  for the Tevatron are consistent with the recent CDF and D0 measurements (21). The relative technicolor corrections to the SM tree-level cross section  $\sigma_0$  are  $\Delta\sigma^{(A)}/\sigma_0 \approx (10 - 36)\%$  for the Tevatron

Table I. Cross sections in Model A at the  $\sqrt{s} = 2$  TeV Tevatron and the  $\sqrt{s} = 14$  TeV LHC with  $M_{\Pi^{0a}}$  varying from 400 GeV to 500 GeV.  $\sigma_0$  denotes the SM tree-level cross section,  $\Delta\sigma^{(A)}$  denotes the correction to  $\sigma_0$ , and  $\sigma_{t\bar{t}}^{(A)} = \sigma_0 + \Delta\sigma^{(A)}$  is the total cross section. All masses are in GeV.

Tevatron			LHC	
$M_{\Pi^{0a}}$	$\Delta\sigma^{(A)}(pb)$	$\sigma_{t\bar{t}}^{(A)}(pb)$	$\Delta\sigma^{(A)}(nb)$	$\sigma_{t\bar{t}}^{(A)}(nb)$
400	2.92	10.94	1.36	2.19
450	1.54	9.56	1.04	1.87
500	0.84	8.86	0.81	1.63

and  $\Delta\sigma^{(A)}/\sigma_0 \approx (98 - 165)\%$  for the LHC, which are quite large due to the  $\Pi^{0a}$  resonance effects. The relative corrections are much larger than those in the  $\gamma\gamma \rightarrow t\bar{t}$  process given in Ref. [5] because of the existence of the  $\Pi^{0a}$  contribution at the hadron colliders. With the integrated luminosities in (20) and assuming a 10% detecting efficiency, we see from Table I that Model A predicts around 2000  $t\bar{t}$  events at the Tevatron and around  $2 \times 10^7$   $t\bar{t}$  events at the LHC. The statistical uncertainty at the 95% C.L. in the case of the Tevatron is then around 4% which is about the same level as the expected systematic error of the  $t\bar{t}$  cross section measurement ( $\sim 5\%$  [25]), and the statistical uncertainty in the case of the LHC is around  $4 \times 10^{-4}$  which is much smaller than the expected systematic error ( $\sim \text{few}\%$  [25]). The relative corrections  $\Delta\sigma^{(A)}/\sigma_0$  from Table I are all larger than the above uncertainties and thus *these events are all experimentally detectable at both the Tevatron and the LHC*. To illustrate the resonances, we further plot the  $t\bar{t}$  invariant mass distributions for  $M_{\Pi^{0a}} = 400$  GeV at the Tevatron and the LHC in Fig. 2(a) and Fig. 2(b), respectively. The resonance effects at  $M_{\Pi^{0a}}$  can be clearly seen. Comparing Fig. 2(a) with the new vector resonances (with the width about 20% of the mass) shown in Ref. [2], we see that the  $\Pi^{0a}$  resonance is sharper.

## B. Results of Model B

The results of the cross sections in Model B at the Tevatron are listed in Table II. Since  $M_{\Pi^0}$  is much lower than the  $t\bar{t}$  threshold, there is almost no  $\Pi^0$  resonance effect, so that we simply take a typical value  $M_{\Pi^0} = 150$  GeV in the calculation. To see the resonance effects of  $\Pi^{0a}$  and  $\Pi_t$  with various values of  $M_{\Pi^{0a}}$  and  $M_{\Pi_t}$ , we take their masses varying in the ranges  $400 \text{ GeV} \lesssim M_{\Pi^{0a}} \lesssim$

$500 \text{ GeV}$  and  $500 \text{ GeV} \lesssim M_{\Pi_t} \lesssim 1 \text{ TeV}$ , respectively. For the parameter  $m'_t$ , we take two typical values  $m'_t = 5$  GeV (denoted by the superscript  $i = 1$ ) and  $m'_t = 15$  GeV (denoted by the superscript  $i = 2$ ), and the cross sections with these two values of  $m'_t$  are denoted by  $\sigma_{t\bar{t}}^{(B1)}$

Table II. Cross sections in Model B at the  $\sqrt{s} = 2$  TeV Tevatron.  $\Delta\sigma^{(Bi)}$  denotes the correction to the SM tree-level cross section  $\sigma_0$ , and  $\sigma_{t\bar{t}}^{(Bi)} = \sigma_0 + \Delta\sigma^{(Bi)}$  is the total cross section. The superscript  $i$  denotes the two cases of  $m'_t = 5$  GeV ( $i = 1$ ) and  $m'_t = 15$  GeV ( $i = 2$ ). All masses are in GeV, and all cross sections are in pb.

$M_{\Pi_t^0}$	$M_{\Pi^{0a}}$	$\Delta\sigma^{(B1)}$	$\sigma_{t\bar{t}}^{(B1)}$	$\Delta\sigma^{(B2)}$	$\sigma_{t\bar{t}}^{(B2)}$
500	400	0.13	8.15	0.47	8.49
500	450	0.11	8.13	0.29	8.31
500	500	0.09	8.11	0.18	8.20
600	400	0.10	8.12	0.44	8.46
600	450	0.08	8.09	0.26	8.28
600	500	0.06	8.08	0.15	8.17
700	400	0.08	8.10	0.42	8.44
700	450	0.06	8.08	0.24	8.26
700	500	0.05	8.06	0.14	8.15
800	400	0.07	8.09	0.42	8.43
800	450	0.05	8.07	0.24	8.25
800	500	0.04	8.06	0.13	8.15
900	400	0.07	8.08	0.41	8.43
900	450	0.05	8.06	0.23	8.25
900	500	0.03	8.05	0.13	8.14
1000	400	0.06	8.08	0.41	8.42
1000	450	0.04	8.06	0.23	8.24
1000	500	0.03	8.05	0.12	8.14

and  $\sigma_{t\bar{t}}^{(B2)}$ , respectively. From the values of  $\sigma_{t\bar{t}}^{(B1)}$  and  $\sigma_{t\bar{t}}^{(B2)}$  in Table II, we see that they are consistent with the recent CDF and D0 measurements (21). We know that the width of a heavy  $\Pi_t$  is rather large due to the largeness of  $(m_t - m'_t)/F_{\Pi_t}$  (the smallness of  $F_{\Pi_t}$ ), thus the cross sections depend more sensitively on  $M_{\Pi^{0a}}$  than on  $M_{\Pi_t}$  as we see in Table II. Moreover, the  $\Pi^{0a}$  couplings are proportional to  $m'_t$ , while the  $\Pi_t$  couplings are proportional to  $m_t - m'_t$ . The former is much sensitive to  $m'_t$  than the latter does since  $m_t \gg m'_t$ . Thus the cross sections with  $m'_t = 15$  GeV are all larger than those with  $m'_t = 5$  GeV in Table II. From Table II we see that all relative corrections  $\Delta\sigma^{(B1)}/\sigma_0$  and  $\Delta\sigma^{(B2)}/\sigma_0$  are at most 6% which is of the same order as the expected systematic error ( $\sim 5\%$ ). Hence *Model B can hardly be detected at the Tevatron*.

The obtained cross sections in Model B at the LHC are listed in Table III. Now the relative corrections  $|\Delta\sigma^{(B1)}|/\sigma_0$  in Table III are around (3 - 7)% depending on the value of  $\Pi_t$ . Since the statistical uncertainty is of the order of  $10^{-4}$  as can be seen from Table III and

Table III. Cross sections in Model B at the  $\sqrt{s} = 14$  TeV LHC.  $\Delta\sigma^{(Bi)}$  denotes the correction to the SM tree level cross sections  $\sigma_0$ , and  $\sigma_{t\bar{t}}^{(Bi)} = \sigma_0 + \Delta\sigma^{(Bi)}$  is the total cross section. The superscript  $i$  denotes the two cases of  $m'_t = 5$  GeV ( $i = 1$ ) and  $m'_t = 15$  GeV ( $i = 2$ ). All masses are in GeV, and all cross sections are in nb.

$M_{\Pi_t^0}$	$M_{\Pi^{0a}}$	$\Delta\sigma^{(B1)}$	$\sigma_{t\bar{t}}^{(B1)}$	$\Delta\sigma^{(B2)}$	$\sigma_{t\bar{t}}^{(B2)}$
500	400	0.06	0.89	0.23	1.05
500	450	0.06	0.88	0.19	1.02
500	500	0.05	0.88	0.15	0.98
600	400	0.05	0.87	0.21	1.04
600	450	0.05	0.87	0.18	1.01
600	500	0.04	0.87	0.14	0.97
700	400	0.04	0.87	0.20	1.03
700	450	0.04	0.86	0.17	1.00
700	500	0.03	0.86	0.13	0.96
800	400	0.04	0.86	0.20	1.03
800	450	0.03	0.86	0.17	0.99
800	500	0.03	0.86	0.13	0.95
900	400	0.03	0.86	0.20	1.02
900	450	0.03	0.86	0.16	0.99
900	500	0.03	0.85	0.12	0.95
1000	400	0.03	0.86	0.19	1.02
1000	450	0.03	0.85	0.16	0.99
1000	500	0.02	0.85	0.12	0.95

eq.(21), the PGB effects for  $m'_t = 5$  GeV in Model B can be marginally detected at the LHC (at least for  $M_{\Pi_t} \lesssim 800$  GeV and  $M_{\Pi^{0a}} \lesssim 450$  GeV). For  $m'_t = 15$  GeV, the relative corrections  $\Delta\sigma^{(B2)}/\sigma_0$  are in the range of (15–27)% which are larger than the systematic error and the statistical uncertainty. Thus the PGB effects for  $m'_t = 15$  GeV in Model B can be clearly detected at the LHC. Comparing the cross sections in Table I and Table III, we see that the relative differences between Model A and Model B at the LHC are  $R_{AB}^{(1)} \equiv (\sigma_{t\bar{t}}^{(A)} - \sigma_{t\bar{t}}^{(B1)})/\sigma_{t\bar{t}}^{(A)} \approx (46-61)\%$  and  $R_{AB}^{(2)} \equiv (\sigma_{t\bar{t}}^{(A)} - \sigma_{t\bar{t}}^{(B2)})/\sigma_{t\bar{t}}^{(A)} \approx (40-53)\%$ . These are all much larger than the systematic error and the statistical uncertainty, so that Model A and Model B can be clearly distinguished at the LHC.

As an illustration, the  $t\bar{t}$  invariant mass distributions in Model B for  $M_{\Pi^{0a}} = 400$  GeV and  $M_{\Pi_t} = 500$  GeV at the Tevatron and the LHC are shown in Fig. 3. Since the width of  $\Pi^{0a}$  in Model B depends on  $m'_t/F_\Pi$  rather than on  $m_t/F_\Pi$ , the resonance of  $\Pi^{0a}$  in Model B is much sharper than that in Model A. This is a clear distinction between Model B and Model A. The width of  $\Pi_t$  is very wide due to the largeness of  $(m_t - m'_t)/F_{\Pi_t}$  (the smallness of  $F_{\Pi_t}$ ). Because of the large width of  $\Pi_t$ , no resonance peak of  $\Pi_t$  can be seen, and the contribution of  $\Pi_t$  is just a slight enhancement of the  $M_{t\bar{t}}$  distribution in a certain region. In Fig. 3(b), the solid curve and the dotted curve denote the  $M_{t\bar{t}}$  distribution with and without the  $\Pi_t$  contribution, respectively. From the difference of these two

curves, we can see the effect of the  $\Pi_t$  contribution. We see that both the  $\Pi^{0a}$  and the  $\Pi_t$  contributions look very different from those of the new heavy vector resonances (with the width about 20% of the mass) shown in Ref. [2].

### C. Results of Model C

The obtained cross sections in Model C at the Tevatron and the LHC are listed in Table IV and Table V, respectively. The cross sections in Table IV are consistent with the CDF and D0 data. In Model C, the decay constant  $F_\Pi$  is much smaller than that in Model B, so that the  $\Pi^{0a}$  and  $\Pi^0$  contributions are enhanced<sup>‡</sup>, and thus the cross sections in Tables IV and V are larger than those in Tables II and III.

Table IV. Cross sections in Model C at the  $\sqrt{s} = 2$  TeV Tevatron.  $\Delta\sigma^{(Ci)}$  denotes the correction to the SM tree-level cross section  $\sigma_0$ , and  $\sigma_{t\bar{t}}^{(Ci)} = \sigma_0 + \Delta\sigma^{(Ci)}$  is the total cross section. The superscript  $i$  denotes the two cases of  $m'_t = 5$  GeV ( $i = 1$ ) and  $m'_t = 15$  GeV ( $i = 2$ ). All masses are in GeV, and all cross sections are in pb.

$M_{\Pi_t^0}$	$M_{\Pi^{0a}}$	$\Delta\sigma^{(C1)}$	$\sigma_{t\bar{t}}^{(C1)}$	$\Delta\sigma^{(C2)}$	$\sigma_{t\bar{t}}^{(C2)}$
500	400	0.50	8.52	3.46	11.48
500	450	0.33	8.35	1.91	9.93
500	500	0.21	8.23	0.99	9.00
600	400	0.48	8.49	3.43	11.45
600	450	0.30	8.32	1.88	9.90
600	500	0.18	8.20	0.96	8.98
700	400	0.46	8.47	3.42	11.44
700	450	0.28	8.30	1.87	9.89
700	500	0.16	8.18	0.95	8.96
800	400	0.45	8.47	3.42	11.43
800	450	0.28	8.29	1.86	9.88
800	500	0.16	8.17	0.94	8.96
900	400	0.44	8.46	3.41	11.43
900	450	0.27	8.29	1.86	9.38
900	500	0.15	8.17	0.94	8.95
1000	400	0.44	8.46	3.41	11.43
1000	450	0.27	8.29	1.86	9.87
1000	500	0.15	8.16	0.93	8.95

From Table IV we see that, at the Tevatron, the relative correction  $\Delta\sigma^{(C1)}/\sigma_0$  is about (2–6)% which is at most of the same order as the expected systematic error, and  $\Delta\sigma^{(C2)}/\sigma_0$  is around (12–43)% which is larger than

<sup>‡</sup>In this paper, we have considered the effect of ideal mixing of  $\Pi^0$  in model C, while this effect is not considered in Ref. [4].

the systematic error and the statistical uncertainty. So that, at the Tevatron, *the PGB effects in Model C for  $m'_t = 5$  GeV can hardly be detected, while those for  $m'_t = 15$  GeV can be clearly detected.* The relative differences  $R_{CB}^{(2)} \equiv (\sigma_{t\bar{t}}^{(C2)} - \sigma_{t\bar{t}}^{(B2)})/\sigma_{t\bar{t}}^{(C2)} \approx (9 - 26)\%$ , so that, for  $m'_t = 15$  GeV, *Model C can be distinguished from Model B at the Tevatron.* However, the relative difference  $R_{CA}^{(2)} \equiv (\sigma_{t\bar{t}}^{(C2)} - \sigma_{t\bar{t}}^{(A)})/\sigma_{t\bar{t}}^{(C2)}$  is at most 5%, therefore, *even for  $m'_t = 15$  GeV, Model C can hardly be distinguished from Model A at the Tevatron.*

Table V. Cross sections in Model C at the  $\sqrt{s} = 14$  TeV LHC.  $\Delta\sigma^{(Ci)}$  denotes the correction to the SM tree level cross sections  $\sigma_0$ , and  $\sigma_{t\bar{t}}^{(Ci)} = \sigma_0 + \Delta\sigma^{(Ci)}$  is the total cross section. The superscript  $i$  denotes the two cases of  $m'_t = 5$  GeV ( $i = 1$ ) and  $m'_t = 15$  GeV ( $i = 2$ ). All masses are in GeV, and all cross sections are in nb.

$M_{\Pi_t^0}$	$M_{\Pi^{0a}}$	$\Delta\sigma^{(C1)}$	$\sigma_{t\bar{t}}^{(C1)}$	$\Delta\sigma^{(C2)}$	$\sigma_{t\bar{t}}^{(C2)}$
500	400	0.22	1.04	1.64	2.47
500	450	0.20	1.02	1.35	2.18
500	500	0.16	0.99	1.02	1.85
600	400	0.20	1.03	1.63	2.45
600	450	0.19	1.01	1.34	2.17
600	500	0.15	0.98	1.01	1.84
700	400	0.19	1.02	1.62	2.45
700	450	0.18	1.00	1.33	2.16
700	500	0.14	0.97	1.00	1.83
800	400	0.19	1.02	1.62	2.44
800	450	0.17	1.00	1.33	2.15
800	500	0.14	0.96	1.00	1.82
900	400	0.19	1.01	1.61	2.44
900	450	0.17	1.00	1.33	2.15
900	500	0.13	0.96	1.00	1.82
1000	400	0.18	1.01	1.61	2.44
1000	450	0.17	0.99	1.32	2.15
1000	500	0.13	0.96	0.99	1.82

From Table V we see that, at the LHC, the relative corrections  $\Delta\sigma^{(C1)}/\sigma_0 \approx (16 - 26)\%$ ,  $\Delta\sigma^{(C2)}/\sigma_0 \approx (120 - 200)\%$ . These are all much larger than the systematic error and the statistical uncertainty. So that *the PGB effects in Model C, for both  $m'_t = 5$  GeV and  $m'_t = 15$  GeV, can be clearly detected at the LHC.* Comparing the cross sections in Table V with those in Table I and Table III, we see that the relative differences are  $R_{AC}^{(1)} \equiv (\sigma_{t\bar{t}}^{(A)} - \sigma_{t\bar{t}}^{(C1)})/\sigma_{t\bar{t}}^{(A)} \approx (40 - 54)\%$ ,  $R_{CB}^{(1)} \equiv (\sigma_{t\bar{t}}^{(C1)} - \sigma_{t\bar{t}}^{(B1)})/\sigma_{t\bar{t}}^{(C1)} \approx (11 - 15)\%$ ,  $R_{CA}^{(2)} \equiv (\sigma_{t\bar{t}}^{(C2)} - \sigma_{t\bar{t}}^{(A)})/\sigma_{t\bar{t}}^{(C2)} \approx (11 - 16)\%$ ,  $R_{CB}^{(2)} \equiv (\sigma_{t\bar{t}}^{(C2)} - \sigma_{t\bar{t}}^{(B2)})/\sigma_{t\bar{t}}^{(C2)} \approx (47 - 58)\%$ . These are all much larger than the systematic error and the statistical uncertainty. So that for both  $m'_t = 5$  GeV and  $m'_t = 15$  GeV, *Model C can be clearly distinguished from Model A and Model B at the LHC.*

For comparison with Fig. 2 and Fig. 3, the corresponding  $t\bar{t}$  invariant mass distributions at the Tevatron and the LHC in Model C are illustrated in Fig. 4. We see that *the resonances of  $\Pi^{0a}$  are significantly wider than those in Model B, and clearly narrower than those in Model A* because the width of  $\Pi^{0a}$  depends on  $m'_t/F_\Pi$ , and the values of  $F_\Pi$  are very different in Model B and Model C. This character shows the clear distinction of the three kinds of TC models. Here we see again that the  $\Pi_t$  contribution does not show up as a resonance peak, and its effect can be seen from the difference between the curve with its contribution (the solid curve) and the curve without its contribution (the dotted curve). The shapes of the  $\Pi^{0a}$  and  $\Pi_t$  contributions in Model C all look very different from those of the new heavy vector reonaces shown in Ref. [2].

## IV. CONCLUSIONS

In this paper, we have studied the pseudo-Goldstone boson contributions to the  $t\bar{t}$  production cross sections at the Fermilab Tevatron Run II and the CERN LHC in various technicolor models, and have examined the possibility of testing and distinguishing different technicolor models in the experiments. We take the Appelquist-Terning one-family walking technicolor model (Model A), the original topcolor-assisted technicolor model (Model B), and the topcolor-assisted multi-scale technicolor model (Model C) as three typical examples of technicolor models with and without topcolor. At the hadron colliders, the  $s$ -channel pseudo-Goldstone boson contributions described in Fig. 1 dominate. In the calculation, the MRS set A' parton distribution functions are used to obtain the  $p(\bar{p}) \rightarrow t\bar{t}$  cross sections, and the pseudo-Goldstone boson masses  $M_{\Pi^{0a}}$  and  $M_{\Pi_t}$  are taken to vary in certain ranges (as discussed in Sec. II) to see the dependence of the cross sections on them. The obtained results are compared with the recent CDF and D0 data on the  $t\bar{t}$  production cross sections at the Tevatron [cf. eq.(21)]. It is shown that all the obtained cross sections at the Tevatron are consistent with the CDF and D0 data.

The results of the calculated cross sections are listed in Table I to Table V. Considering the expected systematic error at the Tevatron and the LHC, and assuming a 10% detecting efficiency, we have the following conclusions:

1. Model A can be clearly detected both at the Tevatron and the LHC.
2. In Model B and Model C, the  $\Pi^{0a}$  couplings are proportional to  $m'_t$  ( $m'_t \ll m_t$ ) rather than to  $m_t$  as in Model A. Therefore the  $\Pi^{0a}$  contributions in Model B and Model C are significantly reduced relative to Model A. This causes the fact that, consid-

ering the expected systematic error and the statistic uncertainty, Model B can hardly be detected at the Tevatron, and model C can be detected at the Tevatron only for large  $m'_t$ , say  $m'_t = 15$  GeV. The situation is much better for the LHC. Model B with  $m'_t = 15$  GeV and Model C (with  $m'_t = 5$  GeV and  $m'_t = 15$  GeV) can all be clearly detected, and Model B with  $m'_t = 5$  GeV can be marginally detected at the LHC.

3. Due to the smallness of  $F_{\Pi_t}$  (the largeness of  $(m_t - m'_t)/F_{\Pi_t}$ ), the width of the  $\Pi_t$  resonance is very large which causes the fact that the cross sections are not so sensitive to the variation of  $M_{\Pi_t}$ .
4. For the detectable cases, all the three kinds of models can be experimentally distinguished by the significant differences of their cross sections. Furthermore, the  $\Pi^{0a}$  resonance peaks in the invariant mass  $M_{t\bar{t}}$  distributions for the three kinds of models are also very different. The width of the  $\Pi^{0a}$  resonance in the three models are:  $\Gamma_{\Pi^{0a}}^{(A)} > \Gamma_{\Pi^{0a}}^{(C)} > \Gamma_{\Pi^{0a}}^{(B)}$ . This can serve as a clear distinction between the three kinds of models.
5. Comparing the present results with the heavy vector resonances (with the width about 20% of the mass) shown in Ref. [2], we see that the  $\Pi^{0a}$  resonances are much sharper and the  $\Pi_t$  contributions do not show up as resonances. The behavior of the present resonances are very different from those heavy vector resonances studied in Ref [2].

In summary, the PGB effects in  $t\bar{t}$  productions at the LHC provide feasible tests of technicolor models including distinguishing different typical models. It is complementary to other tests such as the tests studied in Refs. [2,7,11,13,26].

### Acknowledgment

This work is supported by the National Natural Science Foundation of China, the Fundamental Research Foundation of Tsinghua University, and a special grant from the Ministry of Education of China.

- 
- [1] A.P. Heinson, talk at the XXXIVth Rencontres de Moriond, Electroweak Interactions and Unified Theories, Les Arcs, Savoie, France, 13th-20th March 1999, Fermilab Preprint Fermilab-Conf-99/147-E, hep-ex/9906023.
  - [2] C.T. Hill and S.J. Parke, Phys. Rev. D **49**, 4454 (1994).
  - [3] E. Eichten and K. Lane, Phys. Lett. B **327**, 129 (1994).

- [4] C.-X. Yue, H.-Y. Zhou, Y.-P. Kuang and G.-R. Lu, Phys. Rev. D **55**, 5541 (1997).
- [5] H.-Y. Zhou, Y.-P. Kuang, C.-X. Yue, Hua Wang and Gong-Ru Lu, Phys. Rev. D **57**, 4205 (1998).
- [6] T. Appelquist and J. Terning, Phys. Lett. B **315**, 139 (1993).
- [7] C. T. Hill, Phys. Lett. B **345**, 483 (1995).
- [8] K. Lane, Phys. Lett. B **357**, 624 (1995).
- [9] S. Adler, Phys. Rev. **177**, 2426(1969); J. S. Bell and R. Jackiw, Nuovo Cimento A **60**, 47 (1969).
- [10] V. Lubicz, Nucl. Phys. B **404**, 559 (1993); V. Lubicz and P. Santorelli, *ibid.* B **460**, 3 (1996).
- [11] S. Dimopoulos, S. Raby, and G. L. Kane, Nucl. Phys. B **182**, 77 (1981); J. Ellis, et al. , *ibid.* B **182**, 529 (1981).
- [12] D. Slaven, B.-L. Young, and X.-M. Zhang, Phys. Rev. D **45**, 4349 (1992).
- [13] L. Randall and E. H. Simmons, Nucl. Phys. B **380**, 3 (1992).
- [14] K. Lane, and E. Eichten, Phys. Lett. B **352**, 382 (1995); K. Lane, Phys. Rev. D **54**, 2204 (1996); K. Lane, Proceedings of the 1996 Workshop on Perspectives of Strongly Coupled Gauge Theories, Nagoya, Japan, Boston University Report No. BUHEP-97-8, P.72; R.S. Chivukula, B.A. Dobrescu, and J. Terning, Phys. Lett. B **353**, 289 (1995); D. Kominis, *ibid* **358** 312 (1995); G. Buchalla, G. Burdan, C.T. Hill, and D. Kominis, Phys. Rev. D **53**, 5185 (1996).
- [15] G. Burdman and D. Kominis, Phys. Lett. B **403**, 101 (1997).
- [16] W. Loinaz and T. Takeuchi, Phys. Rev. D **60**, 015005 (1999).
- [17] C.-X. Yue, Y.-P. Kuang, G.-R. Lu, and L.-D. Wan, Phys. Rev. D **52**, 5314 (1995); K. Hagiwara and N. Kitazawa, Phys. Rev. D **52**, 5374 (1995).
- [18] S. Dimopoulos and L. Susskind, Nucl. Phys. B **155**, 237 (1979); E. Eichten and K. Lane, Phys. Lett. B **90**, 125 (1980).
- [19] B. Balaji, Phys. Rev. D **53**, 1699 (1996).
- [20] K. Lane and E. Eichten, Phys. Lett. B **222**, 274 (1989); K. Lane and M. V. Ramana, Phys. Rev. D **44**, 2678 (1991).
- [21] K. Hagiwara and D. Zeppenfeld, Nucl. Phys. **B313**,560(1989); V. Barger, T. Han and D. Zeppenfeld, Phys. Rev. **D41**,2782(1990).
- [22] E. Eichten, I. Hinchliffe, K. Lane and C. Quigg, Rev. Mod. Phys, **56**, 579 (1984).
- [23] A.D. Martin, W.J. Stirling, and R.G. Roberts, Phys. Lett. B **354**, 155 (1995).
- [24] E. Laenen, J. Smith, and W. L. van Neerven, Phys. Lett. **B321**, 254(1994).
- [25] T. M. Liss, Proc. Int. Europhysics Conf. on High Energy Physics, July 27  $\rightarrow$  Aug. 2, 1995, Brussels, Belgium, EPS HEP 1995: 190.
- [26] For example, E. Eichten, K. Lane, and J. Womersley, Phys. Lett. B **405** 305 (1997); K. Lane, Phys. Lett. B **388** 803 (1996); E.H. Simmons, R.S. Chivukula, and J. Terning, Proc. International Symposium on Heavy Flavor and Electroweak Theory, edited by C.-H. Chang and C.-S. Huang (World Scientific, Singapore, 1996) pp.234-243, and references therein.

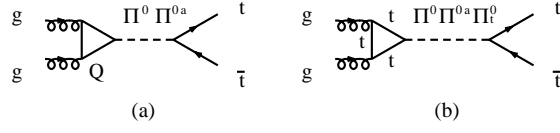


FIG. 1. Feynman diagrams for the  $s$ -channel pseudo-Goldstone boson contributions to the  $p(\bar{p}) \rightarrow t\bar{t}$  productions: (a) the techniquark triangle loop contributions, (b) the top quark triangle loop contributions.

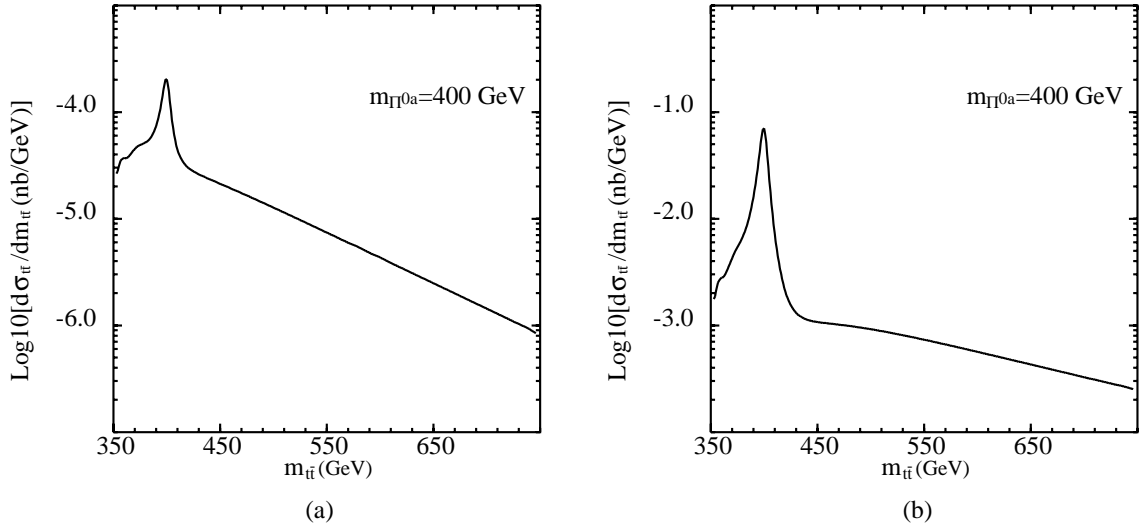


FIG. 2.  $t\bar{t}$  invariant mass distributions for  $M_{\Pi^{0a}} = 400$  GeV in Model A: (a) at the Tevatron, (b) at the LHC.

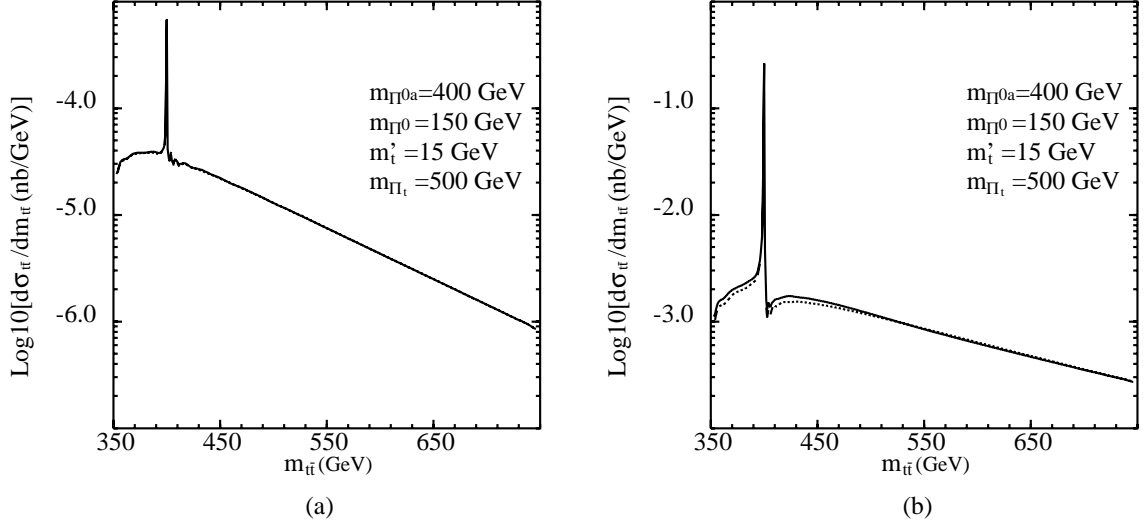


FIG. 3.  $t\bar{t}$  invariant mass distributions for  $M_{\Pi^{0a}} = 400$  GeV and  $M_{\Pi_t} = 500$  GeV in Model B: (a) at the Tevatron, (b) at the LHC. The solid and dotted curves in Fig. 3(b) denote the distributions with and without the  $\Pi_t$  contribution, respectively.

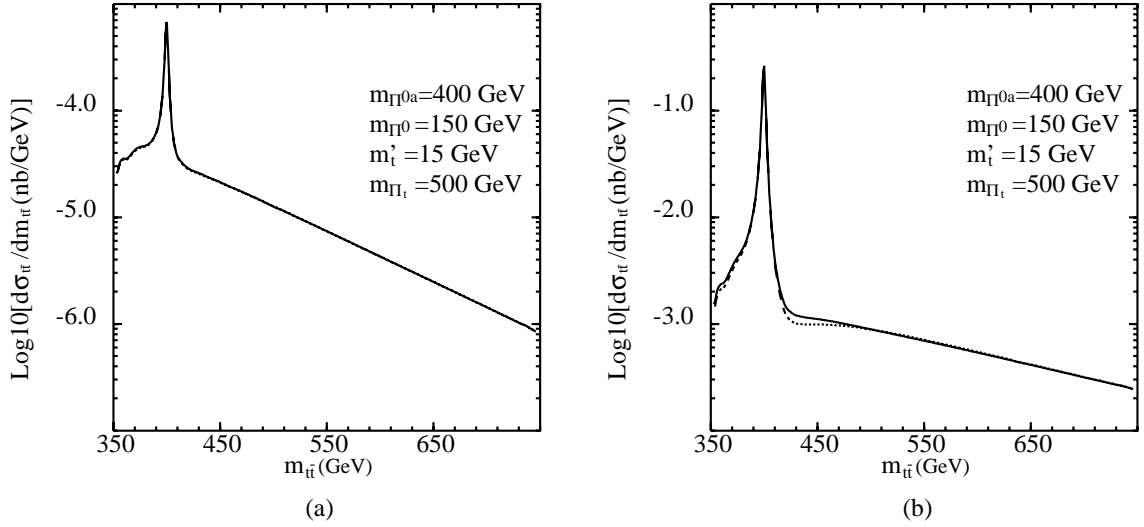


FIG. 4.  $t\bar{t}$  invariant mass distributions for  $M_{\Pi^{0a}} = 400$  GeV and  $M_{\Pi_t} = 500$  GeV in Model C: (a) at the Tevatron, (b) at the LHC. The solid and dotted curves in Fig. 4(b) denote the distributions with and without the  $\Pi_t$  contribution, respectively.